

DNN-Aided Block Sparse Bayesian Learning for User Activity Detection and Channel Estimation in Grant-Free Non-Orthogonal Random Access

Zhaoji Zhang, Ying Li, *Member, IEEE*, Chongwen Huang, Qinghua Guo, *Senior Member, IEEE*, Chau Yuen, *Senior Member, IEEE*, and Yong Liang Guan, *Senior Member, IEEE*

Abstract—In the upcoming Internet-of-Things (IoT) era, the communication is often featured by massive connection, sporadic transmission, and small-sized data packets, which poses new requirements on the delay expectation and resource allocation efficiency of the Random Access (RA) mechanisms of the IoT communication stack. A grant-free non-orthogonal random access (NORA) system is considered in this paper, which could simultaneously reduce the access delay and support more Machine Type Communication (MTC) devices with limited resources. In order to address the joint user activity detection (UAD) and channel estimation (CE) problem in the grant-free NORA system, we propose a deep neural network-aided message passing-based block sparse Bayesian learning (DNN-MP-BSBL) algorithm. In the DNN-MP-BSBL algorithm, the iterative message passing process is transferred from a factor graph to a deep neural network (DNN). Weights are imposed on the messages in the DNN and trained to minimize the estimation error. It is shown that the trained weights could alleviate the convergence problem of the MP-BSBL algorithm, especially on crowded RA scenarios. Simulation results show that the proposed DNN-MP-BSBL algorithm could improve the UAD and CE accuracy with a smaller number of iterations, indicating its advantages for low-latency grant-free NORA systems.

Index Terms—deep neural network, sparse Bayesian learning, grant-free, user activity detection, channel estimation

I. INTRODUCTION

PROVIDING efficient support for the Internet of Things (IoT) and Industry IoT (IIoT) [1] is one of the major objectives for the fifth generation (5G) and the next-generation 6G cellular wireless communication [2]. In order to realize the physical information exchange in IoT, Machine-to-Machine (M2M) communication is anticipated to support billions of Machine Type Communication (MTC) devices [3]. In addition, for most IoT applications such as smart metering and intelligent transportation, the MTC devices are intermittently activated with a low probability, and the size of the data packets transmitted by active devices is relatively small [4], [5]. Therefore, the random access (RA) process for M2M communications in IoT is characterized by massive connection and sporadic transmission, as well as small-sized data packets.

Confronted with the characteristics described above, conventional orthogonal multiple access (OMA) schemes, where orthogonal resource blocks (RBs) are assigned to each device, becomes infeasible due to its extremely low resource efficiency. To address this problem, different RA schemes have been proposed, where activated devices can share or contend for the uplink resources, and these RA schemes can be

generally categorized into two types: grant-based RA [6]–[12] and grant-free RA [13]–[28].

A. Grant-Based Random Access

In grant-based RA schemes, activated users contend for the RBs by transmitting a preamble sequence to BS. At the BS, a RB is assigned to the activated user, whose preamble sequence is received and accepted by the BS.

One problem with the grant-based RA schemes is that the RB is wasted when more than one active device transmit the same preamble sequence. This problem is worsened with the massive connection in crowded RA scenarios. Some solutions were proposed to alleviate the RA congestion by reducing the collision probability, such as the Access Class Barring (ACB) scheme [6], delicate splitting of the RA preamble set [7], and automatic configuration of the RA parameters [8]. Other works addressed the preamble shortage [9], [10] or the early preamble collision detection to avoid RB wastage [11], [12].

However, the RB wastage cannot be fully avoided by grant-based RA schemes, especially in crowded RA scenarios, which results in low resource efficiency. Furthermore, a handshaking process is required between the BS and active devices to recognize the contention winner, which undermines the uplink transmission efficiency of small data packets.

B. Grant-Free Random Access

In grant-free RA schemes, activated users directly transmit data packets with encapsulated pilot sequences over shared uplink resources. Therefore, no grant is required from the BS for uplink transmission, which improves the transmission efficiency, especially for small-sized data packets. Note that in grant-based RA, the BS can acquire the ID of active users during the handshaking process, so that the activity of each user can be easily recognized. By contrast, in grant-free RA, the BS has no priori knowledge of each user's activity before the transmission of data packets. Therefore, it is necessary to exploit encapsulated pilot sequences for user activity detection (UAD) and channel estimation (CE), so that the BS can identify each active user and further accomplish data decoding. Different grant-free RA schemes are explained as follows.

1) *Slotted ALOHA based grant-free RA Schemes*: In slotted ALOHA based grant-free RA schemes, activated devices directly transmit data packets in randomly chosen slots while data packets experiencing no slot collision can be correctly

decoded [13]. In order to improve the throughput of slotted ALOHA protocols, the contention resolution diversity slotted ALOHA (CRDSA) protocol [14] was proposed, where each activated device sends two replicas of the same data packet and successive interference cancellation (SIC) technique is employed to recover the collided replicas. The CRDSA protocol introduced a (2,1) repetition code to the conventional slotted ALOHA protocol while the coded slotted ALOHA (CSA) protocol [15] further combined the general packet erasure codes with SIC. According to the analogy between the channel codes and the data packet replica, the frameless IRSA protocol [16] and the spatially coupled RA protocol [17] were proposed, corresponding to the rateless codes and the spatially coupled LDPC codes, respectively.

Although different modifications have been proposed to improve the throughput of slotted ALOHA protocols, the severe slot collision always leads to the failure of SIC, which hinders the application of slotted ALOHA based protocols in crowded RA scenarios.

2) *Compressed sensing-based grant-free RA schemes:* Due to the sporadic transmission feature of M2M communications, the RA process can be formulated as a sparse signal recovery problem. Therefore, different compressed sensing (CS) algorithms employ pilot sequences to accomplish the user activity detection (UAD) and/or channel estimation (CE) problem. For example, a block CS algorithm [18] was proposed for distributed UAD and resource allocation, based on the clustering of devices. The joint UAD and CE problem was addressed by a modified Bayesian compressed sensing algorithm [19] for the cloud radio access network (C-RAN). In addition, the powerful approximate message passing (AMP) algorithm was employed for the joint UAD and CE problem when the BS is equipped either with a single antenna [20], [21] or with multiple antennas [22], [23].

3) *Sparse Bayesian learning-based grant-free RA schemes:* Different from CS-based RA schemes, the sparse Bayesian learning (SBL) algorithm further considers the prior hyper-parameter of the sparse signal to address the joint UAD and CE problem. The Expectation Maximization (EM) method was employed by the AMP-SBL algorithm [24] to update the sparse signal and the hyper-parameter iteratively. A least square (LS)-based AMP-SBL (LS-AMP-SBL) algorithm [25] was proposed to recover the sparse signal in three steps, i.e., the AMP-SBL first provides a coarse estimate, followed by the derivation for the support of the sparse channel, while the final estimate is derived by the support and the LS estimation. The joint UAD and data decoding task for a grant-free NOMA system was modeled and addressed by a deep auto-encoder in [26], which exploits the prior information of user activation probability and optimizes the choice of spreading signature. However, this auto-encoder is trained based on known channel state information at receiver and a sufficiently static channel, which impedes its application to the rapidly changing environment. Recently, a message-passing receiver design was proposed for the joint channel estimation and data decoding in uplink grant-free SCMA systems [27], exploiting variational Bayesian inference to extract the sparse signals. In addition, a message passing-based block sparse Bayesian learning (MP-

TABLE I
FREQUENTLY USED ABBREVIATIONS AND CORRESPONDING MEANING.

Abbr.	Meaning
DNN	Deep Neural Network
RA	Random Access
NORA	Non-Orthogonal Random Access
UAD	User Activity Detection
CE	Channel Estimation
MP-BSBL [28]	Message Passing-Based Block Sparse Bayesian Learning.
DNN-MP-BSBL	DNN-Aided MP-BSBL
MF	Mean Field
LDS	Low-Density Signature
NMSE	Normalized Mean Square Error

BSBL) algorithm [28] was proposed for a grant-free NOMA system. In both [27] and [28], non-zero elements in the sparse signals are updated with Gaussian message passing [29]–[31] and the hyper-parameters are updated with mean-field (MF) message passing [32].

The Gaussian message passing [29]–[31] is constructed on a factor graph, and it is proven to be optimal on cycle-free graphs. However, this factor graph is densely-connected under crowded RA scenarios, which causes correlated messages and convergence problem for the Gaussian message passing in MP-BSBL algorithm [28]. As a result, the CE and UAD accuracy of the MP-BSBL algorithm is undermined under crowded RA scenarios. To address this problem, we impose weighting parameters on the Gaussian messages and MF message update in the MP-BSBL algorithm. In order to facilitate the training of these weighting parameters, the edge-type message passing process on the factor graph is transformed to a node-type one in the deep neural network (DNN) [33], [34]. Then these weights in the DNN can be trained in a data-driven manner to mitigate the message correlation and the convergence problem in the MP-BSBL algorithm. In this way, higher UAD and CE accuracy can be achieved for crowded RA scenarios.

C. Contributions

In this paper, we focus on an orthogonal frequency division multiplexing system with low-density signature (LDS-OFDM) [35], [36], where devices perform grant-free RA once they are activated. A deep neural network-aided message passing-based block sparse Bayesian learning (DNN-MP-BSBL) algorithm is proposed in this paper to perform joint UAD and CE for the grant-free RA procedure. The iterative message passing process of the MP-BSBL algorithm [28] is transferred from a factor graph to a neural network. Weights are imposed on the messages passing in the neural network and further trained to minimize the estimation error. It is shown that the trained weights could alleviate the convergence problem of the MP-BSBL algorithm, especially in crowded RA scenarios. As a result, the DNN-MP-BSBL algorithm could improve the UAD and CE accuracy with a smaller number of iterations. In addition, the training of the DNN is conducted offline, and negligible online computational complexity is additionally

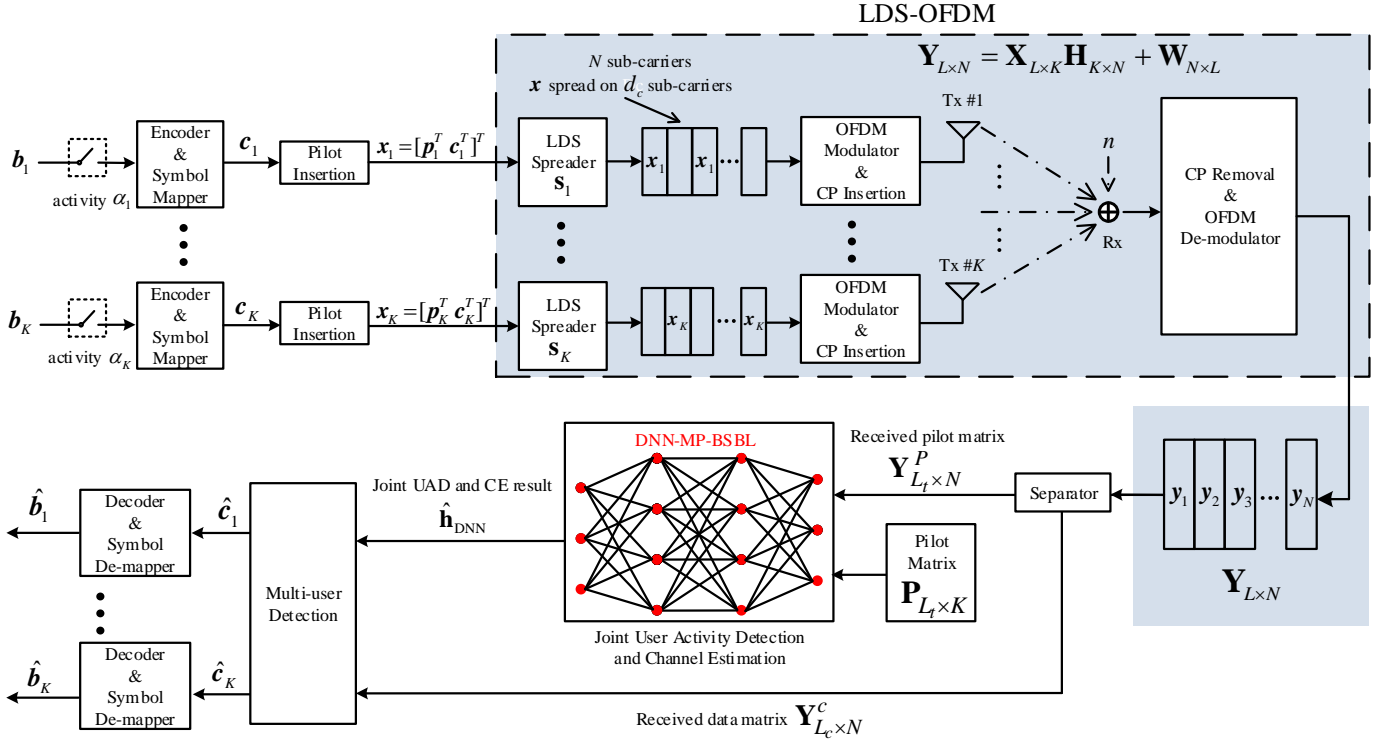


Fig. 1. LDS-OFDM based grant-free NORA system model. The joint UAD and CE problem is solved by the proposed DNN-MP-BSBL algorithm, which processes the first L_t received signals of the pilot sequences, while the MUD module is employed to process the remaining L_c received signals to detect the data transmitted from active users.

sacrificed for the performance improvement by the DNN. This guarantees the feasibility of the proposed DNN-MP-BSBL algorithm for crowded NORA systems with real-time implementation and low-latency requirement.

The rest of this paper is organized as follows. The system model and the MP-BSBL algorithm are presented in Section II. The DNN structure for the DNN-MP-BSBL algorithm is illustrated in Section III, where the weighted message passing is explained in details. Simulation results are given in Section IV to verify the UAD and CE accuracy of the proposed DNN-MP-BSBL algorithm. Finally, Section V concludes this paper. For reading convenience, the frequently-used abbreviations in this paper are summarized in Table. I.

II. JOINT UAD AND CE BY MP-BSBL

A. System Model

As shown in Fig. 1, a LDS-OFDM communication system is considered. It is assumed that there are N sub-carriers and K users, while each user is activated with probability P_a . For each active user k , its binary information sequence \mathbf{b}_k is encoded and further mapped into a QAM symbol sequence $\mathbf{c}_k \in \mathbb{C}^{L_c \times 1}$ with length L_c . One unique pilot sequence \mathbf{p}_k with length L_t is allocated for user k , and \mathbf{p}_k is further inserted into the transmitted symbol sequence \mathbf{x}_k , i.e., $\mathbf{x}_k = [\mathbf{p}_k^T \mathbf{c}_k^T]^T$. Therefore, the length L of \mathbf{x}_k is $L = L_t + L_c$. Then each symbol in \mathbf{x}_k is spread onto d_c sub-carriers, using a low-density spreading pattern \mathbf{s}_k , which is a sparse vector with

length N and d_c non-zero elements. In this way, the same sequence \mathbf{x}_k is transmitted on d_c different sub-carriers.

The LDS spreaders for all the K users are represented by an LDS spreading matrix $\mathbf{S} = [\mathbf{s}_1, \dots, \mathbf{s}_K]$, which is assumed known at the receiver. We consider a regular LDS spreading matrix, i.e., the column degree d_c and the row degree d_r in \mathbf{S} are constant. According to the regular structure of \mathbf{S} , each sub-carrier is shared by d_r potential users, with $d_r = (K/N)d_c$. When multiple users are activated on the same sub-carrier, the grant-free RA procedure is conducted in a non-orthogonal multiple access (NOMA) manner. Therefore, the system model in Fig. 1 is termed a LDS-OFDM based grant-free non-orthogonal random access (NORA) system.

Before transmission, the cyclic prefix (CP) is inserted after the OFDM modulator to avoid the inter-symbol interference (ISI). At the receiver, the CP is removed, and after the OFDM demodulator, we obtain the frequency-domain received signal matrix $\mathbf{Y}_{L \times N} = [\mathbf{y}_1, \dots, \mathbf{y}_n, \dots, \mathbf{y}_N]$, where \mathbf{y}_n is the received signal vector representing the L received symbols on the n -th sub-carrier.

Now we discuss the channel between the input and the output of this LDS-OFDM system. The transmitted sequences of all the K users are organized in an input matrix $\mathbf{X}_{L \times K} = [\mathbf{x}_1, \dots, \mathbf{x}_k, \dots, \mathbf{x}_K]$, while the user activity is equivalently incorporated in the channel matrix $\mathbf{H}_{K \times N}$. Specifically, we consider the *effective* channel gain vector \mathbf{h}_k of user k to integrate the *actual* channel gain vector \mathbf{g}_k with the sparse

spreading pattern \mathbf{s}_k . That is,

$$\begin{aligned} \mathbf{h}_k &= [h_{1k}, \dots, h_{nk}, \dots, h_{Nk}]^T \\ &= [g_{1k}s_{1k}, \dots, g_{nk}s_{nk}, \dots, g_{Nk}s_{Nk}]^T, \end{aligned} \quad (1)$$

where the n -th element g_{nk} of \mathbf{g}_k represents the actual channel gain of user k on the n -th sub-carrier, and the n -th element s_{nk} of \mathbf{s}_k is non-zero if and only if user k chooses to conduct transmission on the n -th sub-carrier. Therefore, the effective channel gain vector \mathbf{h}_k is a sparse vector with d_c non-zero elements. Furthermore, we incorporate user activity in the channel matrix, i.e., $\mathbf{H}_{K \times N} = [\alpha_1 \mathbf{h}_1, \dots, \alpha_K \mathbf{h}_K]^T$, where the activity indicator $\alpha_k = 0$ if user k is inactive. Otherwise, $\alpha_k = 1$. In this way, we can obtain

$$\mathbf{Y}_{L \times N} = \mathbf{X}_{L \times K} \mathbf{H}_{K \times N} + \mathbf{W}_{N \times L}, \quad (2)$$

where $L = L_t + L_c$, the (l, n) -th entry of \mathbf{Y} represents the l -th received symbol on the n -th sub-carrier, the (l, k) -th entry of \mathbf{X} represents the l -th transmitted symbol of the k -th user. The entries in the additive white Gaussian noise (AWGN) matrix \mathbf{W} are assumed i.i.d with noise variance σ_w^2 .

According to the composition of \mathbf{x}_k , \mathbf{Y} can be decomposed as $\mathbf{Y}_{L \times N} = [(\mathbf{Y}_{L_t \times N}^P)^T (\mathbf{Y}_{L_c \times N}^c)^T]^T$, where \mathbf{Y}^P and \mathbf{Y}^c represent the received signal matrices with respect to (w.r.t.) the pilot sequences and the data sequences, respectively. After the separator, \mathbf{Y}^P is further processed by the proposed DNN-MP-BSBL algorithm for the joint UAD and CE. According to the output of the DNN-MP-BSBL algorithm $\hat{\mathbf{h}}_{\text{DNN}}$, \mathbf{Y}^c is fed into the multi-user detection (MUD) module to detect and decode the information bits of active users.

B. Problem Formulation

In this paper, we mainly consider the received pilot matrix \mathbf{Y}^P and solve the joint UAD and CE problem. Analogous to (2), \mathbf{Y}^P can be formulated as

$$\mathbf{Y}_{L_t \times N}^P = \mathbf{P}_{L_t \times K} \mathbf{H}_{K \times N} + \mathbf{W}_{N \times L_t}, \quad (3)$$

where the (l, n) -th entry of \mathbf{Y}^P represents the l -th received signal on the n -th sub-carrier, and the (l, k) -th entry of \mathbf{P} represents the l -th pilot symbol of the k -th user. The pilot matrix \mathbf{P} is assumed known to the receiver. Then we perform vectorization on the transpose of \mathbf{Y}^P as in [28],

$$\begin{aligned} \mathbf{y} &= \text{vec}([\mathbf{Y}^P]^T) = (\mathbf{P} \otimes \mathbf{I}_N) \text{vec}(\mathbf{H}^T) + \mathbf{w} \\ &= \underbrace{\begin{bmatrix} p_{1,1} \mathbf{I}_N & p_{1,2} \mathbf{I}_N & \cdots & p_{1,K} \mathbf{I}_N \\ p_{2,1} \mathbf{I}_N & p_{2,2} \mathbf{I}_N & \cdots & p_{2,K} \mathbf{I}_N \\ \vdots & \vdots & \ddots & \vdots \\ p_{L_t,1} \mathbf{I}_N & p_{L_t,2} \mathbf{I}_N & \cdots & p_{L_t,K} \mathbf{I}_N \end{bmatrix}}_{\mathbf{P}_s} \underbrace{\begin{bmatrix} \alpha_1 \mathbf{h}_1 \\ \alpha_2 \mathbf{h}_2 \\ \vdots \\ \alpha_K \mathbf{h}_K \end{bmatrix}}_{\mathbf{h}_s} + \mathbf{w} \\ &\stackrel{(a)}{=} \underbrace{\bar{\mathbf{P}}}_{\bar{\mathbf{h}}} \begin{bmatrix} \alpha_1 \bar{\mathbf{h}}_1 \\ \alpha_2 \bar{\mathbf{h}}_2 \\ \vdots \\ \alpha_K \bar{\mathbf{h}}_K \end{bmatrix} + \mathbf{w}, \end{aligned} \quad (4)$$

where $\mathbf{P}_s = \mathbf{P} \otimes \mathbf{I}_N$, \otimes represents the Kronecker product, $\mathbf{h}_s = \text{vec}(\mathbf{H}^T)$, and \mathbf{h}_k is the effective channel gain vector of user k on N sub-carriers. According to the LDS spreading matrix \mathbf{S} , the transmitted sequence of each user is only spread onto d_c sub-carriers. Therefore, as explained in (1), $N - d_c$ elements in \mathbf{h}_k are zero, and the positions of the zero elements are known to the BS. We further simplify \mathbf{h}_s by eliminating the zeros according to \mathbf{S} . Accordingly, the columns in \mathbf{P}_s corresponding to the zeros in \mathbf{h}_s are also removed. Finally, we obtain the simplified version of (3) in equation (a) of (4), where $\bar{\mathbf{P}}$ and $\bar{\mathbf{h}}_k$ are obtained from \mathbf{P}_s and \mathbf{h}_k by zero elimination. According to (4), the joint UAD and CE problem is formulated as

$$\begin{aligned} \text{Solve:} & \text{ detect } \alpha_k \text{ and estimate } \bar{\mathbf{h}}_k \text{ if } \alpha_k \text{ is detected as 1, } \forall k \\ \text{Given:} & \text{ } \mathbf{y} \text{ and } \bar{\mathbf{P}} \end{aligned} \quad (5)$$

Remark 1: To enable this joint UAD and CE task, each active user transmits its unique pilot sequence before its data transmission. A common practice is to employ the Zadoff-Chu (ZC) sequences [37] as pilot sequences, which is also considered in this work. One ZC sequence with length L_t is generated as follows,

$$\mathbf{z}_u(n) = \exp\{-i\pi un(n+1)/L_t\}, \quad 0 \leq n < L_t, \quad (6)$$

where $i^2 = -1$, the sequence length L_t is a prime number, and $u \in [1, \dots, L_t - 1]$ is the root of $\mathbf{z}_u(n)$. When the root u is fixed, we can generate $N_u = \lfloor L_t/N_{SF} \rfloor$ different pilot sequences by cyclically shifting one existing sequence by N_{SF} elements. Therefore, when N_{SF} is set to 1, $L_t(L_t - 1)$ different pilot sequences can be generated for the users.

C. MP-BSBL Algorithm [28]

The recovery of the block sparse signal $\bar{\mathbf{h}}$ in (4) can be addressed by the MP-BSBL algorithm [28], which is based on two types of low-complexity message passing algorithms. The Gaussian message passing is employed for updating the estimated channel gain and the mean field (MF) message passing is adopted to approximate the hyper-parameters related to the user activity. The assumptions employed by the MP-BSBL algorithm are detailed as follows.

For user k , the distribution of the channel gains $\bar{\mathbf{h}}_k$ on d_c sub-carriers is assumed conditioned on a hyper-parameter γ_k . Specifically, the channel gains are assumed independently and identically distributed (i.i.d) with complex Gaussian distribution, i.e., $\bar{\mathbf{h}}_k(\gamma_k) \sim \mathcal{CN}(\mathbf{0}, \gamma_k^{-1} \mathbf{I}_{d_c})$. In addition, the reciprocal of the estimated hyper-parameter is compared with a pre-defined threshold γ_{th} to determine the user activity. If $\hat{\gamma}_k^{-1}$ is smaller than γ_{th} , this user is detected as inactive. Otherwise, this user is detected as active. The hyper-parameter γ_k is assumed to follow a Gamma distribution [27], [28], [38]. The noise precision $\lambda = 1/\sigma_w^2$ is unknown at the receiver but assumed with a priori probability $p(\lambda)$. With these assumptions above, the joint a posterior probability is factorized as follows

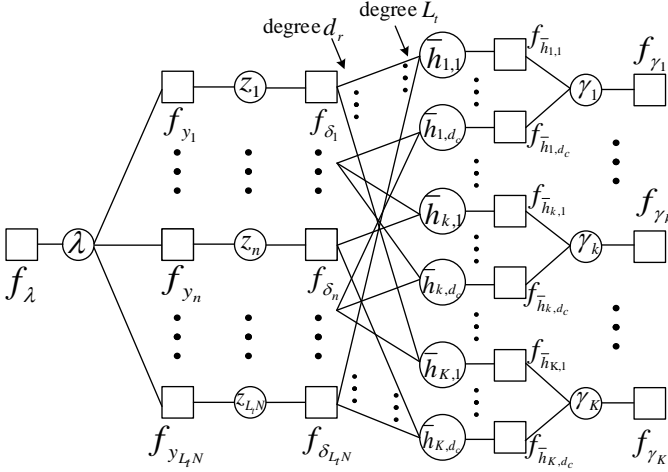


Fig. 2. Factor graph for the message passing in the MP-BSBL algorithm [28].

$$\begin{aligned}
 p(\bar{\mathbf{h}}, \gamma, \lambda | \mathbf{y}) &\propto p(\mathbf{y} | \bar{\mathbf{h}}, \lambda) p(\bar{\mathbf{h}} | \gamma) p(\lambda) p(\gamma) \\
 &= p(\lambda) \prod_{n=1}^{L_t N} p(y_n | \bar{\mathbf{h}}, \lambda) \prod_{k=1}^K \prod_{d=1}^{d_c} p(\bar{h}_{k,d} | \gamma_k) p(\gamma_k),
 \end{aligned} \quad (7)$$

where $p(\lambda) \propto 1/\lambda$, $p(y_n | \bar{\mathbf{h}}, \lambda) = \mathcal{CN}(y_n; \bar{\mathbf{p}}_n^T \bar{\mathbf{h}}, \lambda^{-1})$, $\bar{\mathbf{p}}_n^T$ is the n -th row of matrix $\bar{\mathbf{P}}$ in (4), $p(\bar{h}_{k,d} | \gamma_k) = \mathcal{CN}(\bar{h}_{k,d}; 0, \gamma_k^{-1})$, $p(\gamma_k) = Ga(\gamma_k; a_k, b_k)$, and $p(\gamma) = \prod_{k=1}^{d_c} p(\gamma_k)$, $\mathcal{CN}(x; \mu, \sigma^2)$ represents the complex Gaussian distribution probability density function (pdf) of x with mean μ and variance σ^2 , while $Ga(x; a, b)$ represents the Gamma distribution pdf of x with parameters a and b . According to the variational Bayesian inference theory [38], the parameters a and b are usually assumed in the order of 10^{-4} . Further details are referred to [27], [28].

According to the factorization in (7), a factor graph can be established for the MP-BSBL algorithm, which is illustrated in Fig. 2. In Fig. 2, $f(\lambda)$, $f_{\bar{h}_{k,d}}(\bar{h}_{k,d}, \gamma_k)$, $f_{\gamma_k}(\gamma_k)$ and $f_{y_n}(\bar{\mathbf{h}}, \lambda)$ denote $p(\lambda)$, $p(\bar{h}_{k,d} | \gamma_k)$, $p(\gamma_k)$, and $p(y_n | \bar{\mathbf{h}}, \lambda)$, respectively. In addition, the extra variable $z_n = \bar{\mathbf{p}}_n^T \bar{\mathbf{h}}$ is introduced and the constraint $\delta(z_n - \bar{\mathbf{p}}_n^T \bar{\mathbf{h}})$ is represented by f_{δ_n} . Then, f_{y_n} is a function of z_n and λ , i.e., $f_{y_n}(z_n, \lambda) = \mathcal{CN}(y_n; z_n, \lambda^{-1})$. The MP-BSBL algorithm performed on the factor graph in Fig. 2 is briefed as follows

Denote l as the iteration index and $Q_{k,d}$ as the product of all the incoming messages from the neighboring nodes $\delta_{n'}$ to $\bar{h}_{k,d}$, then according to $Q_{k,d}$, the variance $v_{Q_{k,d}}$ and mean $m_{Q_{k,d}}$ of $\bar{h}_{k,d}$ are derived as follows,

$$v_{Q_{k,d}}^l \approx \left(\sum_{n' \in \mathcal{N}(\bar{h}_{k,d})} \frac{|\bar{P}_{n',kd}|^2}{(\hat{\lambda}^{l-1})^{-1} + v_{\delta_{n' \rightarrow z_{n'}}}^{l-1}} \right)^{-1} \quad (8)$$

$$m_{Q_{k,d}}^l \approx v_{Q_{k,d}}^l \sum_{n' \in \mathcal{N}(\bar{h}_{k,d})} \frac{\bar{P}_{n',kd}^H (y_{n'} - m_{\delta_{n' \rightarrow z_{n'}}}^{l-1})}{(\hat{\lambda}^{l-1})^{-1} + v_{\delta_{n' \rightarrow z_{n'}}}^{l-1}} + m_{\bar{h}_{k,d}}^{l-1} \quad (9)$$

By considering the message $\hat{\gamma}_k^{l-1}$ passing from $f_{\bar{h}_{k,d}}$ to $\bar{h}_{k,d}$, the variance $v_{\bar{h}_{k,d}}^l$ and mean $m_{\bar{h}_{k,d}}^l$ of $\bar{h}_{k,d}$ are updated as

$$v_{\bar{h}_{k,d}}^l = \frac{1}{(v_{Q_{k,d}}^l)^{-1} + \hat{\gamma}_k^{l-1}} \quad (10)$$

$$m_{\bar{h}_{k,d}}^l = \frac{m_{Q_{k,d}}^l}{1 + v_{Q_{k,d}}^l \hat{\gamma}_k^{l-1}}$$

The variance $v_{\delta_n \rightarrow z_n}$ and mean $m_{\delta_n \rightarrow z_n}$ passing from δ_n to z_n are derived in (11).

$$\begin{aligned}
 v_{\delta_n \rightarrow z_n}^l &\approx \sum_{\{i,j\} \in \mathcal{N}(f_{\delta_n})} |\bar{P}_{n,ij}|^2 v_{\bar{h}_{i,j}}^l \\
 m_{\delta_n \rightarrow z_n}^l &\approx \sum_{\{i,j\} \in \mathcal{N}(f_{\delta_n})} \bar{P}_{n,ij} m_{\bar{h}_{i,j}}^l - \frac{v_{\delta_n \rightarrow z_n}^l (y_n - m_{\delta_n \rightarrow z_n}^{l-1})}{(\hat{\lambda}^{l-1})^{-1} + v_{\delta_n \rightarrow z_n}^{l-1}}
 \end{aligned} \quad (11)$$

Then the hyper-parameter $\hat{\gamma}_k^l$ for the variance of the channel gain is updated according to the MF message passing,

$$\hat{\gamma}_k^l = \frac{a_k + d_c + 1}{b_k + \sum_{d=1}^{d_c} \left(|m_{\bar{h}_{k,d}}^l|^2 + v_{\bar{h}_{k,d}}^l \right)} \quad (12)$$

The variance $v_{z_n}^l$ and mean $m_{z_n}^l$ of z_n are derived by $v_{\delta_n \rightarrow z_n}$, $m_{\delta_n \rightarrow z_n}$ and the noise precision $\hat{\lambda}^{l-1}$,

$$\begin{aligned}
 v_{z_n}^l &= \left(\hat{\lambda}^{l-1} + (v_{\delta_n \rightarrow z_n}^l)^{-1} \right)^{-1} \\
 m_{z_n}^l &= v_{z_n}^l \left(y_n \hat{\lambda}^{l-1} + \frac{m_{\delta_n \rightarrow z_n}^l}{v_{\delta_n \rightarrow z_n}^l} \right)
 \end{aligned} \quad (13)$$

Finally, the noise precision $\hat{\lambda}^l$ is updated with the MF message passing,

$$\hat{\lambda}^l = \frac{L_t N}{\sum_{n=1}^{L_t N} \left[(m_{z_n}^l - y_n)^2 + v_{z_n}^l \right]} \quad (14)$$

At the last iteration, if $(\hat{\gamma}_k^l)^{-1}$ is smaller than a predefined threshold γ_{th} , user k is regarded as inactive. Otherwise, this user is determined as active and $\{m_{\bar{h}_{k,d}}^l, d = 1, \dots, d_c\}$ is the estimated channel gain for user k . Further details of the derivations above are referred to [28].

III. DNN-AIDED MP-BSBL ALGORITHM

Two types of message passing are adopted by the MP-BSBL algorithm. The Gaussian message passing is employed for CE in (10), while the MF message passing is employed to update the hyper-parameters $\hat{\gamma}_k^l$ in (12) for UAD. According to the factor graph in Fig. 2, the variable nodes $\bar{h}_{k,d}$ and sum nodes f_{δ_n} are densely connected. That is, the connection between $\bar{h}_{k,d}$ and f_{δ_n} is characterized by many short cycles with girth 4, which results in the correlation problem of the Gaussian messages [29]. Furthermore, in crowded NORA systems, where the number of sum nodes f_{δ_n} is much smaller than the number of variable nodes $\bar{h}_{k,d}$, the correlated Gaussian messages further lead to the convergence problem for the

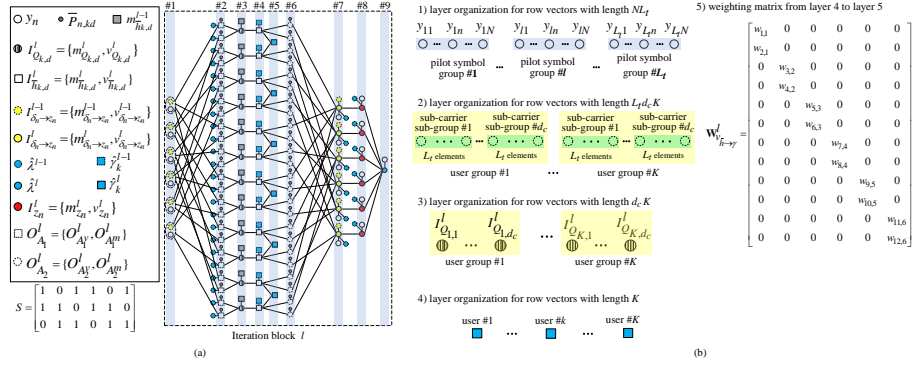


Fig. 3. DNN for the weighted message passing in DNN-MP-BSBL algorithm with $(N = 3, K = 6, L_t = 2, d_c = 2)$ and layer organization.

MP-BSBL algorithm. As a result, the convergence speed is deteriorated and the accuracy of the MP-BSBL algorithm fails to get improved as the signal-to-noise ratio (SNR) increases. On the other hand, the correlated Gaussian messages also lead to inaccuracy for the MF message update, which undermines the UAD performance.

Confronted with the problems above, we propose a DNN-MP-BSBL algorithm, which imposes weights on the Gaussian messages on the factor graph in Fig. 2. Simultaneously, weights are also imposed on the MF message update in (12) and further trained to improve the UAD accuracy. To facilitate the training of the weights, we transfer the message passing process from the factor graph in Fig. 2 to a DNN structure. The back-and-forth message passing process on the factor graph is now transformed into a forward-propagation trellis in Fig. 3(a), which resembles the structure of a neural network. It is assumed that there are $N = 3$ sub-carriers, $K = 6$ users, the length of pilot sequence is $L_t = 2$, each user chooses $d_c = 2$ sub-carriers to perform uplink data transmission, and the DNN-MP-BSBL algorithm is performed with N_{it} iterations. The regular LDS spreading matrix \mathbf{S} is also shown in Fig. 3(a).

As shown in Fig. 3(a), the trellis can be considered as a neural network. Each iteration of the MP-BSBL algorithm is now represented by one iteration block. Since the structure is identical for each iteration block, we only illustrate one iteration block in Fig. 3(a). However, it is noted that neighboring iteration blocks are connected. For illustration simplicity, we include the nodes from the $(l-1)$ -th iteration block, e.g. $\mathbf{I}_{\delta_n \rightarrow z_n}^{l-1}$ and $\hat{\lambda}^{l-1}$ as the input nodes in the l -th iteration block. In this way, the entire DNN is constructed by connecting N_{it} iteration blocks. Within each iteration block, one layer represents one particular message, i.e., each layer is defined by its output message. Two auxiliary layers A_1 and A_2 , i.e., Layer 2 and Layer 6 are also added for the clarity of illustration. Therefore, according to equations (8) to (14), there are 9 layers within each iteration block. Detailed organization of each layer

TABLE II
INPUT AND OUTPUT FOR EACH LAYER OF THE DNN.

Index	Layer Input	Layer Output	Length
1	None	$\mathbf{y}, \mathbf{I}_{\delta \rightarrow z}^{l-1} = \{v_{\delta \rightarrow z}^{l-1}, m_{\delta \rightarrow z}^{l-1}\}$	NL_t
2	$\mathbf{y}, \mathbf{I}_{\delta \rightarrow z}^{l-1}, \hat{\lambda}^{l-1}, \mathbf{P}$	$\mathbf{O}_{A_1}^l = \{O_{A_1}^l, O_{A_1^m}^l\}$	$L_t d_c K$
3	$\mathbf{m}_h^{l-1}, \mathbf{O}_{A_1}^l$	$\mathbf{I}_Q^l = \{v_Q^l, m_Q^l\}$	$d_c K$
4	$\mathbf{I}_Q^l, \hat{\lambda}^{l-1}$	$\mathbf{I}_h^l = \{v_h^l, m_h^l\}$	$d_c K$
5	\mathbf{I}_h^l	$\hat{\lambda}^l$	K
6	$\mathbf{P}, \mathbf{I}_h^l$	$\mathbf{O}_{A_2}^l = \{O_{A_2}^l, O_{A_2^m}^l\}$	$L_t d_c K$
7	$\mathbf{y}, \mathbf{I}_{\delta \rightarrow z}^{l-1}, \hat{\lambda}^{l-1}, \mathbf{O}_{A_2}^l$	$\mathbf{I}_{\delta \rightarrow z}^l = \{v_{\delta \rightarrow z}^l, m_{\delta \rightarrow z}^l\}$	NL_t
8	$\mathbf{y}, \hat{\lambda}^{l-1}, \mathbf{I}_{\delta \rightarrow z}^l$	$\mathbf{I}_z^l = \{v_z^l, m_z^l\}$	NL_t
9	$\mathbf{I}_z^l, \mathbf{y}$	$\hat{\lambda}^l$	1

is illustrated in Fig. 3(b) and the weighted message passing process is explained as follows.

A. Layer Organization and Weighting Matrix

For notational simplicity, the nodes in each layer are placed in a row vector in Fig. 3(b), and the weighted message passing process is then equivalent to the input vector multiplying a weighting matrix. The input vectors, output vector, and the length of output vector for each layer are listed in Table II while the elements of different vectors are organized as follows.

1) *For vectors with length NL_t :* The organization for the row vector \mathbf{y} in Layer 1 is taken as an example in Fig. 3(b). Every N elements are grouped into a pilot symbol group according to the common pilot symbol they correspond to.

These L_t pilot symbol groups are organized according to the index of the pilot symbols. Within each pilot symbol group, the N elements are organized according to the sub-carrier index. For example, the n -th node y_{ln} in the l -th pilot symbol group represents the l -th received pilot signal on the n -th sub-carrier. In this way, the row vector \mathbf{y} is organized as $\mathbf{y} = [y_{11}, \dots, y_{1N}, \dots, y_{L_t1}, \dots, y_{L_tN}]$.

2) *For vectors with length $L_t d_c K$* : The organization for the auxiliary row vector $\mathbf{O}_{A_2}^l$ in Layer 6 is taken as an example. Every $L_t d_c$ elements are grouped into a user group, according to the common user they correspond to. Within each user group, every L_t elements are grouped into a sub-group according to the common sub-carrier they correspond to. Within each sub-carrier sub-group, the L_t elements are arranged according to the pilot symbol index.

3) *For vectors with length $d_c K$* : The organization for the row vector \mathbf{I}_Q^l in Layer 3 is taken as an example. Every d_c elements are grouped together according to the common user they correspond to. Within each user group, the d_c elements are organized according to the sub-carrier index. In this way, the row vector \mathbf{I}_Q^l is organized as $\mathbf{I}_Q^l = [I_{Q,1,1}^l, \dots, I_{Q,1,d_c}^l, \dots, I_{Q,K,1}^l, \dots, I_{Q,K,d_c}^l]$, where $I_{Q,k,d}^l = \{m_{Q,k,d}^l, v_{Q,k,d}^l\}$.

4) *For vectors with length K* : The K elements in the row vector $\hat{\gamma}^l$ are arranged according to the user index.

5) *Weighting matrix*: Since input vectors and output vector of a layer are organized as row vectors, the weighted message update (i.e., the output vector) for every layer can be represented by the input vector multiplied by a weighting matrix. The size of the weighting matrix is $L_I \times L_O$ where L_I and L_O are the length of the input vector and the output vector, respectively. According to Fig. 3(a), nodes in neighboring layers are not fully connected, i.e., the weighting matrix is defined by the inter-layer connection. An example is shown in Fig. 3(b) for the weighting matrix defined by the connection from Layer 4 to Layer 5 of Fig. 3(a). According to this example, the (i, j) -th entry of the weighting matrix is non-zero if and only if the i -th node in the input layer is connected to the j -th node in the output layer. Furthermore, only the non-zero weights in the weighting matrix are trained for the DNN-MP-BSBL algorithm.

B. Weighted Message Passing

The weighted message passing is explained as follows.

Layer 1: Layer 1 serves as the input of the neural network within one iteration block and it is composed of two message vectors, $\mathbf{y} = \{y_n, \forall n\}$ and $\mathbf{I}_{\delta \rightarrow z}^{l-1} = \{v_{\delta \rightarrow z}^{l-1}, m_{\delta \rightarrow z}^{l-1}\} = \{v_{\delta_n \rightarrow z_n}^{l-1}, m_{\delta_n \rightarrow z_n}^{l-1}, \forall n\}$. The elements y_n and $I_{\delta_n \rightarrow z_n}^{l-1} = \{v_{\delta_n \rightarrow z_n}^{l-1}, m_{\delta_n \rightarrow z_n}^{l-1}\}$ are grouped together in Fig. 3(a) since they share identical connection to the nodes in Layer 2.

Layer 2: Layer 2 is the auxiliary layer A_1^l , and the output $\mathbf{O}_{A_1}^l$ is composed of two message vectors $\mathbf{O}_{A_1^v}^l$ and $\mathbf{O}_{A_1^m}^l$, whose elements correspond to the terms in the cumulative summation of (8) and (9), respectively. The weighted message update of Layer 2 is derived as follows,

$$\mathbf{O}_{A_1^v}^l = \frac{\mathbf{P}^2}{\frac{1}{\lambda^{l-1}} \times \mathbf{W}_{\lambda \rightarrow A_1^v}^l + \mathbf{v}_{\delta \rightarrow z}^{l-1} \times \mathbf{W}_{v_{\delta \rightarrow z}^l \rightarrow A_1^v}^l} \quad (15)$$

$$\mathbf{O}_{A_1^m}^l = \frac{\mathbf{P}^H \cdot * \left(\mathbf{y} \times \mathbf{W}_{y \rightarrow A_1^m}^l - \mathbf{m}_{\delta \rightarrow z}^{l-1} \times \mathbf{W}_{m_{\delta \rightarrow z}^l \rightarrow A_1^m}^l \right)}{\frac{1}{\lambda^{l-1}} \times \mathbf{W}_{\lambda \rightarrow A_1^m}^l + \mathbf{v}_{\delta \rightarrow z}^{l-1} \times \mathbf{W}_{v_{\delta \rightarrow z}^l \rightarrow A_1^m}^l} \quad (16)$$

where $\mathbf{P}^2 = \{|\bar{P}_{n,k,d}|^2, \forall n, k, d\}$ and $\mathbf{P}^H = \{\bar{P}_{n,k,d}^H, \forall n, k, d\}$ are row vectors with length $L_t d_c K$. $\mathbf{W}_{\lambda \rightarrow A_1^v}^l$ and $\mathbf{W}_{\lambda \rightarrow A_1^m}^l$ are two weighting matrices with size $1 \times L_t d_c K$. $\mathbf{W}_{v_{\delta \rightarrow z}^l \rightarrow A_1^v}^l$, $\mathbf{W}_{y \rightarrow A_1^m}^l$, $\mathbf{W}_{m_{\delta \rightarrow z}^l \rightarrow A_1^m}^l$, and $\mathbf{W}_{v_{\delta \rightarrow z}^l \rightarrow A_1^m}^l$ are weighting matrices defined by the connection from Layer 1 to Layer 2. In addition, the fraction and $\cdot *$ operations are the element-wise division and multiplication operations while the \times operation refers to the matrix multiplication operation.

Layer 3: The weighted output message vectors $\mathbf{I}_Q^l = \{v_Q^l, m_Q^l\} = \{v_{Q,k,d}^l, m_{Q,k,d}^l, \forall k, d\}$ of Layer 3 are derived as follows,

$$\mathbf{v}_Q^l = \frac{1}{\mathbf{O}_{A_1^v}^l \times \mathbf{W}_{A_1^v \rightarrow v_Q}^l} \\ \mathbf{m}_Q^l = \mathbf{v}_Q^l \cdot * \left(\mathbf{O}_{A_1^m}^l \times \mathbf{W}_{A_1^m \rightarrow m_Q}^l \right) + \mathbf{m}_h^{l-1} \times \mathbf{W}_{h \rightarrow Q}^l \quad (17)$$

where $\mathbf{W}_{A_1^v \rightarrow v_Q}^l$ and $\mathbf{W}_{A_1^m \rightarrow m_Q}^l$ are weighting matrices defined by the connection from Layer 2 to Layer 3. $\mathbf{W}_{h \rightarrow Q}^l$ is a diagonal weighting matrix with size $d_c K \times d_c K$.

Layer 4: The weighted output message vectors $\mathbf{I}_h^l = \{v_h^l, m_h^l\} = \{v_{h,k,d}^l, m_{h,k,d}^l, \forall k, d\}$ of Layer 4 are derived as follows,

$$\mathbf{v}_h^l = \frac{1}{\frac{1}{v_Q} + (\hat{\gamma}^{l-1} \otimes \mathbf{1}_{d_c}) \times \mathbf{W}_\gamma^l} \\ \mathbf{m}_h^l = \frac{\mathbf{m}_Q^l}{\mathbf{1}_{d_c K} \times \mathbf{W}_{\text{one} \rightarrow h} + \left(\mathbf{v}_Q^l \cdot * (\hat{\gamma}^{l-1} \otimes \mathbf{1}_{d_c}) \right) \times \mathbf{W}_{v_Q \rightarrow h}^l} \quad (18)$$

where \otimes refers to the Kronecker product. $\mathbf{1}_{d_c}$ and $\mathbf{1}_{d_c K}$ are two all-one row vectors and their vector length are d_c and $d_c K$, respectively. \mathbf{W}_γ^l , $\mathbf{W}_{\text{one} \rightarrow h}$, and $\mathbf{W}_{v_Q \rightarrow h}^l$ are diagonal weighting matrices with size $d_c K \times d_c K$.

Layer 5: The weighted output message vector $\hat{\gamma}^l = \{\hat{\gamma}_k^l, \forall k\}$ is derived as follows,

$$\hat{\gamma}^l = \frac{\mathbf{a} + d_c + 1}{\mathbf{b} + |\mathbf{m}_h^l|^2 \times \mathbf{W}_{m_h \rightarrow \gamma}^l + \mathbf{v}_h^l \times \mathbf{W}_{v_h \rightarrow \gamma}^l} \quad (19)$$

where $\mathbf{a} = \{a_k, \forall k\}$ and $\mathbf{b} = \{b_k, \forall k\}$ are row vectors with length K , $|\mathbf{m}_h^l|^2 = \{|m_{h,k,d}^l|^2, \forall k, d\}$, $\mathbf{W}_{m_h \rightarrow \gamma}^l$ and $\mathbf{W}_{v_h \rightarrow \gamma}^l$ are weighting matrices defined by the connection from Layer 4 to Layer 5.

Layer 6: Layer 6 is the auxiliary layer A_2^l with weighted output message vectors $\mathbf{O}_{A_2^v}^l$ and $\mathbf{O}_{A_2^m}^l$, whose elements correspond to the terms in the cumulative summation in (11).

$$\mathbf{O}_{A_2^v}^l = \mathbf{P}^2 \cdot * \mathbf{v}_h^l \\ \mathbf{O}_{A_2^m}^l = \mathbf{P} \cdot * \mathbf{m}_h^l \quad (20)$$

where $\mathbf{P} = \{\bar{P}_{n,k,d}, \forall n, k, d\}$ is a row vector with length

$L_t d_c K$.

Layer 7: The weighted output vectors $\mathbf{I}_{\delta \rightarrow z}^l = \{\mathbf{v}_{\delta \rightarrow z}^l, \mathbf{m}_{\delta \rightarrow z}^l\} = \{v_{\delta_n \rightarrow z_n}^l, m_{\delta_n \rightarrow z_n}^l, \forall n\}$ of Layer 7 are derived as follows,

$$\begin{aligned} \mathbf{v}_{\delta \rightarrow z}^l &= \mathbf{O}_{A_2^v}^l \times \mathbf{W}_{A_2^v \rightarrow v_\delta}^l \\ \mathbf{m}_{\delta \rightarrow z}^l &= \mathbf{O}_{A_2^m}^l \times \mathbf{W}_{A_2^m \rightarrow m_\delta}^l \\ &\quad - \frac{\mathbf{v}_{\delta \rightarrow z}^l * \left(\mathbf{y} \times \mathbf{W}_{y \rightarrow \delta}^l - \mathbf{m}_{\delta \rightarrow z}^{l-1} \times \mathbf{W}_{m_\delta \rightarrow m_\delta}^l \right)}{\left(\hat{\lambda}^{l-1} \right)^{-1} \times \mathbf{W}_{\lambda \rightarrow \delta}^l + \mathbf{v}_{\delta \rightarrow z}^{l-1} \times \mathbf{W}_{v_\delta \rightarrow m_\delta}^l} \end{aligned} \quad (21)$$

where $\mathbf{W}_{A_2^v \rightarrow v_\delta}^l$ and $\mathbf{W}_{A_2^m \rightarrow m_\delta}^l$ are weighting matrices defined by the connection from Layer 6 to Layer 7. $\mathbf{W}_{y \rightarrow \delta}^l$, $\mathbf{W}_{m_\delta \rightarrow m_\delta}^l$ and $\mathbf{W}_{v_\delta \rightarrow m_\delta}^l$ are diagonal weighting matrices with size $NL_t \times NL_t$. $\mathbf{W}_{\lambda \rightarrow \delta}^l$ is a weighting matrix with size $1 \times NL_t$.

Layer 8: The weighted output vectors $\mathbf{I}_z^l = \{\mathbf{v}_z^l, \mathbf{m}_z^l\} = \{v_{z_n}^l, m_{z_n}^l, \forall n\}$ of Layer 8 are derived as follows,

$$\begin{aligned} \mathbf{v}_z^l &= \frac{1}{\hat{\lambda}^{l-1} \times \mathbf{W}_{\lambda \rightarrow z}^l + \frac{1}{\mathbf{v}_{\delta \rightarrow z}^l} \times \mathbf{W}_{v_\delta \rightarrow v_z}^l} \\ \mathbf{m}_z^l &= \mathbf{v}_z^l * \left(\left(\mathbf{y} * \hat{\lambda}^{l-1} \right) \times \mathbf{W}_{y \rightarrow z}^l + \frac{\mathbf{m}_{\delta \rightarrow z}^l}{\mathbf{v}_{\delta \rightarrow z}^l} \times \mathbf{W}_{m_\delta \rightarrow v_z}^l \right) \end{aligned} \quad (22)$$

where $\mathbf{W}_{v_\delta \rightarrow v_z}^l$ and $\mathbf{W}_{m_\delta \rightarrow v_z}^l$ are weighting matrices defined by the connection from Layer 7 to Layer 8. $\mathbf{W}_{y \rightarrow z}^l$ is a diagonal weighting matrix with size $NL_t \times NL_t$, and $\mathbf{W}_{\lambda \rightarrow z}^l$ is a weighting matrix with size $1 \times NL_t$.

Layer 9: The weighted output message $\hat{\lambda}^l$ of Layer 9 is derived as follows,

$$\hat{\lambda}^l = \frac{L_t N}{\left(\mathbf{m}_z^l \times \mathbf{W}_{m_z \rightarrow \lambda}^l - \mathbf{y} \times \mathbf{W}_{y \rightarrow \lambda}^l \right)^2 \times \mathbf{1}_{NL_t}^T + \mathbf{v}_z^l \times \mathbf{W}_{v_z \rightarrow \lambda}^l} \quad (23)$$

where $\mathbf{W}_{m_z \rightarrow \lambda}^l$ and $\mathbf{W}_{y \rightarrow \lambda}^l$ are diagonal weighting matrices with size $NL_t \times NL_t$, and $\mathbf{1}_{NL_t}^T$ is an all-one column vector with length NL_t . $\mathbf{W}_{v_z \rightarrow \lambda}^l$ is a weighting matrix with size $NL_t \times 1$.

C. Loss Function

The DNN-MP-BSBL algorithm is conducted in two periods: the training period and the testing period. In the training period, according to the given samples in the training set, the non-zero entries in the weighting matrices are trained to minimize the estimation error. In the testing period, the weighting matrices are fixed. The UAD and CE accuracy of the DNN-MP-BSBL algorithm is evaluated by the samples in the test set.

In order to train the non-zero entries in the weighting matrices, a loss function is employed during the training period to measure the estimation error. Then the weights are adjusted with the stochastic gradient descent (SGD) algorithm in a back-propagation manner to minimize the loss function. For the stability of the SGD algorithm, we employ the mean square error (MSE) $\|\hat{\mathbf{h}}_{\text{DNN}} - \mathbf{h}\|_2^2$ as the loss function, where $\hat{\mathbf{h}}_{\text{DNN}}$ is

Algorithm 1 DNN-MP-BSBL algorithm

Input: \mathbf{y} , $\bar{\mathbf{P}}$, N_{it} , d_c ,

trained weighting matrices in equations (15) to (23)

Output: $\hat{\mathbf{h}}_{\text{DNN}}$, the index set of active user IDX

Initialize:

$$l = 0; \hat{\lambda}^l = 10^3; \hat{\gamma}^l = \mathbf{1};$$

$$\mathbf{v}_{\delta \rightarrow z}^l = \mathbf{1}, \mathbf{m}_{\delta \rightarrow z}^l = \mathbf{0}; \mathbf{m}_h^l = \mathbf{0}.$$

for $l = 1 : N_{it}$ **do**

1. With $\hat{\lambda}^{l-1}$, \mathbf{m}_h^{l-1} , $\mathbf{v}_{\delta \rightarrow z}^{l-1}$, and $\mathbf{m}_{\delta \rightarrow z}^{l-1}$ in the $(l-1)$ -th iteration, update \mathbf{v}_Q^l and \mathbf{m}_Q^l by (15), (16), and (17).
2. With \mathbf{v}_Q^l , \mathbf{m}_Q^l in the l -th iteration and $\hat{\gamma}^{l-1}$ in the $(l-1)$ -th iteration, update \mathbf{v}_h^l and \mathbf{m}_h^l by (18).
3. With \mathbf{v}_h^l and \mathbf{m}_h^l in the l -th iteration, update $\hat{\gamma}^l$ by (19).
4. With $\hat{\lambda}^{l-1}$, $\mathbf{v}_{\delta \rightarrow z}^{l-1}$, $\mathbf{m}_{\delta \rightarrow z}^{l-1}$ in the $(l-1)$ -th iteration and \mathbf{v}_h^l , \mathbf{m}_h^l in the l -th iteration, update $\mathbf{v}_{\delta \rightarrow z}^l$ and $\mathbf{m}_{\delta \rightarrow z}^l$ by (20) and (21).
5. With $\hat{\lambda}^{l-1}$ in the $(l-1)$ -th iteration and $\mathbf{v}_{\delta \rightarrow z}^l$, $\mathbf{m}_{\delta \rightarrow z}^l$ in the l -th iteration, update \mathbf{v}_z^l and \mathbf{m}_z^l by (22).
6. With \mathbf{v}_z^l and \mathbf{m}_z^l in the l -th iteration, update the noise precision $\hat{\lambda}^l$ by (23).

return:

$$\text{IDX} = \text{find} \left(\{ \{ \hat{\gamma}_k^l \}^{-1} \} > \gamma_{th} \right),$$

$$\hat{\mathbf{h}}_{\text{DNN}} = \{ \mathbf{0}, k \notin \text{IDX} \} \cup \{ m_{h_{k,d}}^l, k \in \text{IDX}, d = 1, \dots, d_c \}.$$

the estimated channel gain and \mathbf{h} is the known channel gain in the training set. It is noted that, different from the training period, the Normalized MSE (NMSE) $\|\hat{\mathbf{h}}_{\text{DNN}} - \mathbf{h}\|_2^2 / \|\mathbf{h}\|_2^2$ is considered for the simulations in the testing period to measure the UAD and CE accuracy.

D. Summary of the Proposed DNN-MP-BSBL Algorithm

After the training period, all the weighting matrices are fixed, and the proposed DNN-MP-BSBL algorithm is summarized in Algorithm 1. After N_{it} iterations, the UAD decision is made by comparing $\left(\hat{\gamma}_k^{N_{it}} \right)^{-1}$ with a threshold γ_{th} . If $\left(\hat{\gamma}_k^{N_{it}} \right)^{-1} \leq \gamma_{th}$, user k is detected as inactive. Otherwise, this user is detected as active and $\{ m_{h_{k,d}}^{N_{it}}, \forall d \}$ is the estimated channel gain for user k .

E. Computational Complexity

It is emphasized that the weighting matrices are trained off-line, so that we can neglect the training complexity in the training period. Instead, we only focus on the online computational complexity of the DNN-MP-BSBL algorithm in the testing period. In addition, if all the non-zero entries in the weighting matrices are fixed as 1, the DNN-MP-BSBL algorithm is identical to the MP-BSBL algorithm, whose complexity was thoroughly investigated in [28]. Therefore, we first present the computational complexity of the MP-BSBL algorithm as a benchmark.

TABLE III
EXTRA NUMBER OF MULTIPLICATIONS Δ_{\times} CAUSED BY WEIGHTING
MATRICES IN DNN-MP-BSBL ALGORITHM.

Weighting Matrix	Eqn	Δ_{\times}
$\mathbf{W}_{\lambda \rightarrow A_1^v}^l, \mathbf{W}_{\lambda \rightarrow A_1^m}^l, \mathbf{W}_{v_{\delta} \rightarrow A_1^v}^l, \mathbf{W}_{v_{\delta} \rightarrow A_1^m}^l$	(15),(16)	$L_t d_c K$
$\mathbf{W}_{y \rightarrow A_1^m}^l, \mathbf{W}_{m_{\delta} \rightarrow A_1^m}^l$	(16)	0
$\mathbf{W}_{A_1^v \rightarrow v_Q}^l, \mathbf{W}_{A_1^m \rightarrow m_Q}^l$	(17)	0
$\mathbf{W}_{\bar{h} \rightarrow Q}^l$	(17)	$2d_c K$
$\mathbf{W}_{\gamma}^l, \mathbf{W}_{v_{\gamma} \rightarrow \bar{h}}^l$	(18)	$d_c K$
$\mathbf{W}_{\text{one} \rightarrow \bar{h}}$	(18)	0
$\mathbf{W}_{m_{\bar{h}} \rightarrow \gamma}^l, \mathbf{W}_{v_{\bar{h}} \rightarrow \gamma}^l$	(19)	$d_c K$
$\mathbf{W}_{A_2^v \rightarrow v_{\delta}}^l, \mathbf{W}_{A_2^m \rightarrow m_{\delta}}^l$	(21)	0
$\mathbf{W}_{y \rightarrow \delta}^l, \mathbf{W}_{m_{\delta} \rightarrow m_{\delta}}^l, \mathbf{W}_{v_{\delta} \rightarrow m_{\delta}}^l, \mathbf{W}_{\lambda \rightarrow \delta}^l$	(21)	$L_t N$
$\mathbf{W}_{y \lambda \rightarrow z}^l, \mathbf{W}_{m v \rightarrow z}^l, \mathbf{W}_{\lambda \rightarrow z}^l, \mathbf{W}_{v_{\delta} \rightarrow v_z}^l$	(22)	$L_t N$
$\mathbf{W}_{m_z \rightarrow \lambda}^l, \mathbf{W}_{y \rightarrow \lambda}^l$	(23)	$2L_t N$
$\mathbf{W}_{v_z \rightarrow \lambda}^l$	(23)	$L_t N$

In each iteration of the MP-BSBL algorithm, a total number of $(10L_t + 10)Kd_c + (7d_r + 14)L_t N + K + 2$ multiplications are required. Specifically, $(10L_t + 8)Kd_c$ multiplications are required for the calculation of $v_{h_{k,d}}^l$ and $m_{h_{k,d}}^l$ in (10), $(7d_r + 4)L_t N$ multiplications for $v_{\delta_n \rightarrow z_n}^l$ and $m_{\delta_n \rightarrow z_n}^l$ in (11), $(2d_c + 1)K$ multiplications for $\hat{\gamma}_k^l$ in (12), $8L_t N$ multiplications for $v_{z_n}^l$ and $m_{z_n}^l$ in (13), and $2L_t N + 2$ multiplications for $\hat{\lambda}^l$ in (14).

Compared with the MP-BSBL algorithm, the DNN-MP-BSBL algorithm incurs extra computational complexity when multiplying the non-zero weights in the weighting matrices. Then we analyze the number of extra multiplications, denoted by Δ_{\times} , that is caused by each weighting matrix. Related results are listed in Table. III. Note that in Table. III, some weighting matrices will not lead to extra multiplications. For example, the weighting matrix $\mathbf{W}_{A_1^v \rightarrow v_Q}^l$ imposed on $\mathbf{O}_{A_1^v}^l$ in (17) is equivalently imposed on \mathbf{P}^2 in (15). Therefore, we can replace \mathbf{P}^2 with $\mathbf{P}^2 \times \mathbf{W}_{A_1^v \rightarrow v_Q}^l$ in (15), and remove $\mathbf{W}_{A_1^v \rightarrow v_Q}^l$ from (17). In this way, $\Delta_{\times} = 0$ for $\mathbf{W}_{A_1^v \rightarrow v_Q}^l$, and we can have the same results for $\mathbf{W}_{y \rightarrow A_1^m}^l$ and $\mathbf{W}_{m_{\delta} \rightarrow A_1^m}^l$ in (16) and $\mathbf{W}_{A_1^m \rightarrow m_Q}^l$ in (17), as well as $\mathbf{W}_{A_2^v \rightarrow v_{\delta}}^l$ and $\mathbf{W}_{A_2^m \rightarrow m_{\delta}}^l$ in (21). In addition, we have $\Delta_{\times} = 0$ for $\mathbf{W}_{\text{one} \rightarrow \bar{h}}$ in (18) since it serves as an additive bias term in the DNN, instead of a multiplicative weighting term. Furthermore, the weighting matrices in the first row of Table. III are imposed on the auxiliary layer A_1^l , which is far from the output of each iteration block. Therefore, the weights in these weighting matrices have negligible impacts on the final output, and we can fix these non-zero weights as 1 to reduce the computational complexity of the DNN-MP-BSBL algorithm.

According to the analysis, the DNN-MP-BSBL algorithm incurs $6Kd_c + 13L_t N$ extra multiplications compared with the MP-BSBL algorithm. That is, a total of $(10L_t + 16)Kd_c +$

$(7d_r + 27)L_t N + K + 2$ multiplications are required by the DNN-MP-BSBL algorithm in each iteration, which is only slightly larger than that of the low-complexity MP-BSBL algorithm. For example, according to the configurations in Table. IV, the DNN-MP-BSBL algorithm increases the computational complexity by only 4.3%, compared with the MP-BSBL algorithm. In addition, we also present the computational complexity of the BOMP estimator [28] and the LS-AMP-BSL estimator [25], which are investigated for comparison in Section IV-C. The overall number of multiplications in the BOMP estimator is $K^+ L_t d_c K + \frac{(K^+ + 1)K^+}{2} L_t d_c (N + 1) + \frac{[(K^+ + 1)K^+]^2 d_c^3}{4}$, while that for the LS-AMP-BSL estimator is $N_{it}((9L_t + 11)Kd_c + (7d_r + 4)L_t N) + K^+ L_t d_c (N + 1) + (K^+ d_c)^3$, where K^+ is the number of active users. It is shown that the complexity of the BOMP estimator and the LS-AMP-BSL estimator increases with the square or cube of K^+ . By contrast, the complexity of the DNN-MP-BSBL algorithm only increases linearly with K .

IV. SIMULATIONS

For the simulations, we consider a crowded NORA system with low-latency requirement, which is a common scenario for ultra-reliable low-latency communication (URLLC) and massive MTC (mMTC) applications in 5G and IoT. The congestion degree of the NORA system is characterized by the number of active users on each sub-carrier, which is proportional to the ratio $\frac{K}{N}$. Without loss of any generality, we assume a small number of available sub-carriers, i.e., $N = 8$ to simulate the crowded RA scenarios with limited uplink resources. Other parameters related to the simulations and the DNN are listed in Table IV.

In order to satisfy the low-latency requirement, we investigate the UAD and CE accuracy of the DNN-MP-BSBL algorithm with a small number of iterations, i.e., $N_{it} \leq 20$. For comparison, the NMSE performances of the LS-AMP-BSL estimator [25], the BOMP estimator (with known active user number) [28] and the GA-MMSE estimator (with known user activity) are also provided. The NMSE performance of GA-MMSE estimator serves as the lower bound. It is shown that the proposed DNN-MP-BSBL algorithm could guarantee lower NMSE for CE and better UAD accuracy within a feasible number of iterations.

A. Convergence

The convergence performances of the proposed DNN-MP-BSBL algorithm and the MP-BSBL algorithm [28] are illustrated in Fig. 4, with different number of iterations and different SNR. Also included is the NMSE of the GA-MMSE estimator. It is shown in Fig. 4 that for a small number of iterations, the MP-BSBL algorithm converges slowly and exhibits limited improvement for higher SNR. By contrast, the proposed DNN-MP-BSBL algorithm exhibits better NMSE performance and faster convergence. For different SNR, the DNN-MP-BSBL algorithm with 10 iterations could achieve the same NMSE as the MP-BSBL algorithm with 20 iterations. With 20 iterations, the DNN-MP-BSBL algorithm could closely approach the lower bound, and the gaps to the bound

TABLE IV
RELATED PARAMETERS FOR SIMULATIONS

Parameter	Symbol	Value
User number	K	110
Subcarrier number	N	8
Pilot length	L_t	11
Spreading factor	d_c	4
Activation probability for each user	P_a	0.1
UAD threshold	γ_{th}	0.1
Size of training set		10^5
Size of test set		10^5
Size of mini-batch		200
Epoch number		20
Learning rate		10^{-3}

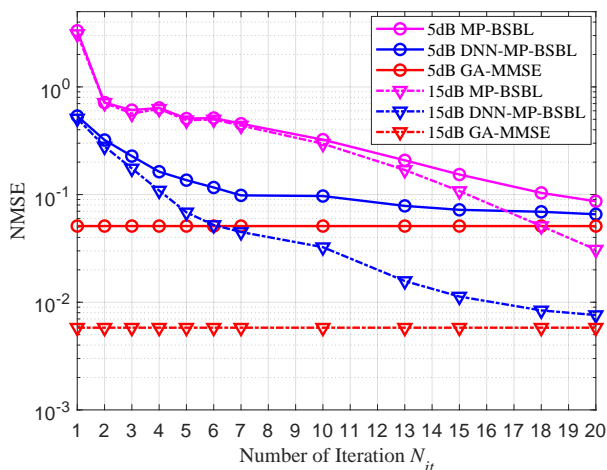


Fig. 4. Convergence with iteration for the proposed DNN-MP-BSBL algorithm and the MP-BSBL algorithm [28].

are 1.3×10^{-2} and 1.7×10^{-3} for SNR=5dB and 15dB, respectively. In addition, the improvement by the DNN-MP-BSBL algorithm is more prominent with a higher SNR. For example, the DNN-MP-BSBL algorithm could improve the NMSE performance of the MP-BSBL algorithm by almost one magnitude order when SNR=15dB.

B. CE and UAD Accuracy With Different P_a

The NMSE performance of the proposed DNN-MP-BSBL algorithm is investigated with different activation probability P_a , and the simulation results are illustrated in Fig. 5. It is shown that when P_a increases, the NORA system is crowded with more active users. As a result, the NMSE performance deteriorates for both the DNN-MP-BSBL algorithm and the MP-BSBL algorithm. In addition, the NMSE performance of the MP-BSBL algorithm shows no improvement when SNR increases from 10dB to 16dB. By contrast, the proposed DNN-MP-BSBL algorithm could always guarantee improvement on the NMSE performance with different SNR and different P_a . Particularly, the improvement is more prominent with lower P_a and higher SNR. For example, the DNN-MP-BSBL

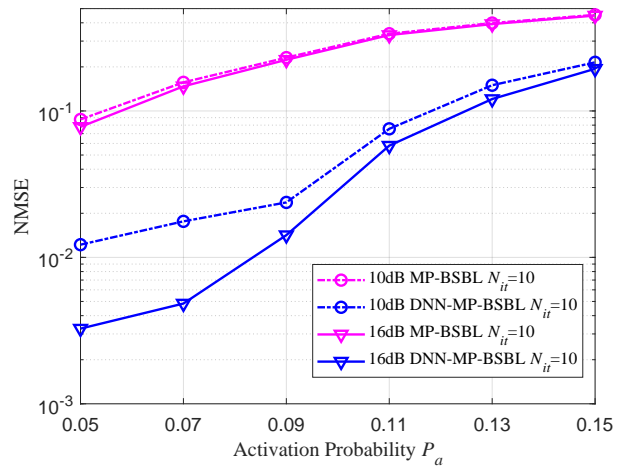


Fig. 5. NMSE performance for the proposed DNN-MP-BSBL algorithm and the MP-BSBL algorithm [28] with different activation probability P_a .

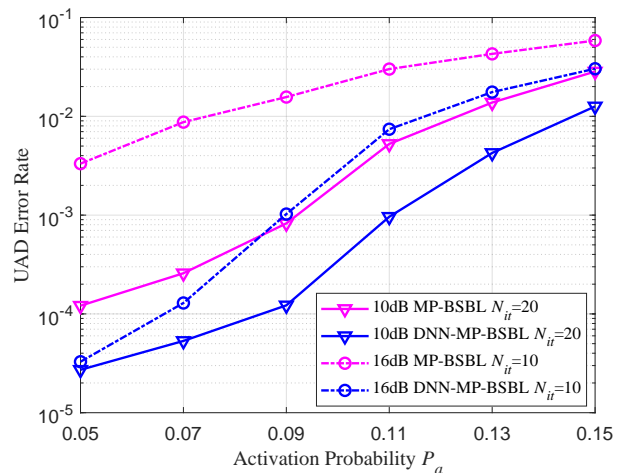


Fig. 6. UAD accuracy for the proposed DNN-MP-BSBL algorithm and the MP-BSBL algorithm [28] with different activation probability P_a .

algorithm could improve the NMSE by almost one magnitude order when SNR=10dB and P_a is relatively low. Furthermore, the NMSE can be further lowered by the DNN-MP-BSBL algorithm when SNR increases to 16dB.

In the DNN-MP-BSBL algorithm, weights are also imposed on the MF message update in (19) to alleviate the influence of correlated Gaussian messages and improve the UAD accuracy. We also investigate the UAD accuracy of the DNN-MP-BSBL algorithm with different P_a , and the results are shown in Fig. 6. It is shown that the proposed DNN-MP-BSBL algorithm could improve the UAD accuracy of the MP-BSBL algorithm for different P_a , SNR, and different number of iterations. Similarly, this improvement on UAD accuracy is more prominent when P_a is relatively low and SNR is high. For example, the DNN-MP-BSBL algorithm could improve the UAD error rate by two magnitude orders when SNR=16dB and $P_a \leq 0.1$.

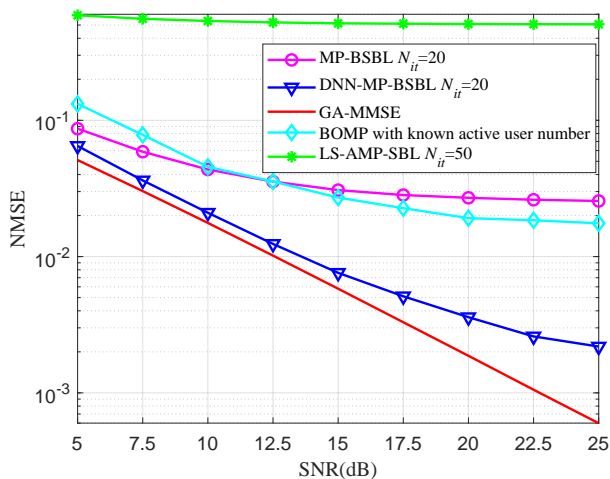


Fig. 7. NMSE performance for CE with different SNR.

C. CE Accuracy With Different SNR

Finally, we compare the proposed DNN-MP-BSBL algorithm with the LS-AMP-BSL estimator [25], the BOMP estimator (with known active user number) [28], and the GA-MMSE estimator (with known user activity). The simulation results are illustrated in Fig. 7 and the NMSE performance of the GA-MMSE estimator serves as the lower bound.

As shown in Fig. 7, in crowded NORA systems, both the MP-BSBL algorithm and the BOMP estimator diverge from the NMSE lower bound as SNR increases, and the LS-AMP-SBL algorithm fails to work even with 50 iterations. By contrast, the DNN-MP-BSBL algorithm could closely approach the lower bound within a wide range of SNR. Therefore, the DNN-MP-BSBL algorithm requires fewer iterations and provides better NMSE performance, indicating its advantages in crowded NORA system with low-latency requirement.

V. CONCLUSIONS

A DNN-MP-BSBL algorithm was proposed in this paper for the joint UAD and CE problem in grant-free NORA systems. The iterative message passing process is transferred from a factor graph to a DNN, while weights are imposed on the messages and trained to improve the UAD and CE accuracy. It was verified that the weighted message passing in the DNN-MP-BSBL algorithm could alleviate the convergence problem of the MP-BSBL algorithm in crowded NORA systems. Simulation results showed that the NMSE performance of the DNN-MP-BSBL algorithm could approach the lower bound in a feasible number of iterations, indicating its advantages for low-latency NORA systems.

REFERENCES

- [1] L. D. Xu, W. He, and S. Li, "Internet of Things in industries: a survey," *IEEE Transactions on Industrial Informatics*, vol. 10, no. 4, pp. 2233-2243, Nov. 2014.
- [2] W. Saad, M. Bennis, and M. Chen, "A vision of 6G wireless systems: applications, trends, technologies, and open research problems." [Online]. Available: <https://arxiv.org/abs/1902.10265>

- [3] A. Osseiran, V. Braun, T. Hidekazu, P. Marsch, H. Schotten, H. Tullberg, M. A. Uusitalo, and M. Schellman, "The foundation of the mobile and wireless communications system for 2020 and beyond: challenges, enablers and technology solutions," *2013 IEEE 77th Vehicular Technology Conference (VTC Spring)*, June 2013.
- [4] 3GPP, "Service Requirements for Machine-Type Communications," TS 22.368 V13.1.0, Dec. 2014.
- [5] G. Wu, S. Talwar, K. Johnsson, N. Himayat, and K. D. Johnson, "M2M: From mobile to embedded internet," *IEEE Commun. Mag.*, vol. 49, no. 4, pp. 36-43, April 2011.
- [6] Z. Wang and V. W. S. Wong, "Optimal access class barring for stationary machine type communication devices with timing advance information," *IEEE Trans. Wireless Commun.*, vol. 14, no. 10, pp. 5374-5387, Oct. 2015.
- [7] K.-D. Lee, S. Kim, and B. Yi, "Throughput comparison of random access methods for M2M service over LTE networks," *Proc. 2011 IEEE GLOBECOM Wkshps.*, Dec. 2011, pp. 373-377.
- [8] S. Choi, W. Lee, D. Kim, K. J. Park, S. Choi, and K. Y. Han, "Automatic configuration of random access channel parameters in LTE systems," *Proc. 2011 IFIP Wireless Days*, Oct. 2011, pp. 1-6.
- [9] H. S. Jang, S. M. Kim, H.-S. Park, and D. K. Sung, "Enhanced spatial group based random access for cellular M2M communications," *IEEE International Conference on Communication Workshop (ICCW)*, London, UK, June 2015, pp. 2102-2107.
- [10] T. Kim, H. S. Jang, and D. K. Sung, "An enhanced random access scheme with spatial group based reusable preamble allocation in cellular M2M networks," *IEEE Commun. Lett.*, vol. 19, no. 10, pp. 1714-1717, Oct. 2015.
- [11] H. S. Jang, S. M. Kim, H. S. Park, and D. K. Sung, "An early preamble collision detection scheme based on tagged preambles for cellular M2M random access," *IEEE Transactions on Vehicular Technology*, vol. 66, no. 7, pp. 5974-5984, July 2017.
- [12] Z. Alavikia and A. Ghasemi, "Collision-aware resource access scheme for LTE-based Machine-to-Machine communications," *IEEE Transactions on Vehicular Technology*, vol. 67, no. 5, pp. 4683-4688, May 2018.
- [13] L. G. Roberts, "ALOHA packet system with and without slots and capture," *ACM SIGCOMM Comput. Commun. Rev.*, vol. 5, no. 2, pp. 28-42, 1975.
- [14] E. Casini, R. De Gaudenzi, and O. del Rio Herrero, "Contention resolution diversity slotted ALOHA (CRDSA): An enhanced random access scheme for satellite access packet networks," *IEEE Trans. Wireless Commun.*, vol. 6, no. 4, pp. 1408-1419, Apr. 2007.
- [15] E. Paolini, G. Liva, and M. Chiani, "Coded slotted ALOHA: a graph-based method for uncoordinated multiple access," *IEEE Trans. Inf. Theory*, vol. 61, no. 12, pp. 6815-6832.
- [16] C. Stefanovic, P. Popovski, and D. Vukobratovic, "Frameless ALOHA protocol for wireless networks," *IEEE Commun. Lett.*, vol. 16, no. 12, pp. 2087-2090.
- [17] G. Liva, E. Paolini, M. Lentmaier, and M. Chiani, "Spatially-coupled random access on graphs," *IEEE Inter. Symp. Inf. Theory (ISIT)*, Cambridge, MA, 2012, pp. 478-482.
- [18] Y. Chang, P. Jung, C. Zhou, and S. Stanczak, "Block compressed sensing based distributed device detection and resource allocation for M2M communications," *IEEE International Conference on Acoustics, Speech and Signal Processing (ICASSP)*, Mar. 2016, pp. 3791-3795.
- [19] X. Xu, X. Rao, and V. K. N. Lau, "Active user detection and channel estimation in uplink CRAN systems," *IEEE Inter. Conf. Commun. (ICC)*, June 2015, pp. 2727-2732.
- [20] G. Hannak, M. Mayer, A. Jung, G. Matz, and N. Goertz, "Joint channel estimation and activity detection for multiuser communication systems," *IEEE Inter. Conf. Commun. (ICC) Workshop*, June 2015, pp. 2086-2091.
- [21] Z. Chen and W. Yu, "Massive device activity detection by approximate message passing," in *IEEE Inter. Conf. Acoustics, Speech, Signal Processing (ICASSP)*, Mar. 2017, pp. 3514-3518.
- [22] L. Liu and W. Yu, "Massive connectivity with massive MIMO-part I: device activity detection and channel estimation," *IEEE Transactions on Signal Processing*, vol. 66, no. 11, pp. 2933-2946.
- [23] L. Liu and W. Yu, "Massive connectivity with massive MIMO-part II: achievable rate characterization," *IEEE Transactions on Signal Processing*, vol. 66, no. 11, pp. 2947-2959.
- [24] M. Al-Shoukairi and B. Rao, "Sparse Bayesian learning using approximate message passing," *48th Asilomar Conference on Signals, Systems and Computers*, 2014, pp. 1957-1961.
- [25] C. Wei, H. Liu, Z. Zhang, J. Dang, and L. Wu, "Near-optimum sparse channel estimation based on least squares and approximate message passing," *IEEE Wireless Communications Letters*, vol. 6, no. 6, pp. 754-757.

- [26] N. Ye, X. Li, H. Yu, A. Wang, W. Liu, and X. Hou, "Deep learning aided grant-free NOMA towards reliable low-latency access in tactile Internet of Things," *IEEE Transactions on Industrial Informatics*.
- [27] F. Wei, W. Chen, Y. Wu, J. Ma, and T. A. Tsiftsis, "Message-passing receiver design for joint channel estimation and data decoding in uplink grant-free SCMA systems," *IEEE Trans. Wireless Commun.*, vol. 18, no. 1, pp. 167-181, Jan. 2019.
- [28] Y. Zhang, Q. Guo, Z. Wang, J. Xi, and N. Wu, "Block sparse Bayesian learning based joint user activity detection and channel estimation for grant-free NOMA systems," *IEEE Transactions on Vehicular Technology*, vol. 67, no. 10, pp. 9631-9640.
- [29] L. Liu, C. Yuen, Y. L. Guan, Y. Li, and Y. Su, "Convergence analysis and assurance for Gaussian message passing iterative detector in massive MU-MIMO systems," *IEEE Trans. Wireless Commun.*, vol. 15, no. 9, pp. 6487-6500.
- [30] C. Huang, L. Liu, C. Yuen and S. Sun, "Iterative channel estimation using LSE and sparse message passing for MmWave MIMO systems," *IEEE Transactions on Signal Processing*, vol. 67, no. 1, pp. 245-259, 1 Jan. 2019.
- [31] C. Huang, L. Liu and C. Yuen, "Asymptotically optimal estimation algorithm for the sparse signal with arbitrary distributions," *IEEE Transactions on Vehicular Technology*, vol. 67, no. 10, pp. 10070-10075, Oct. 2018.
- [32] E. Riegler, G. E. Kirkelund, C. N. Manchon, M. Badiu, and B. H. Fleury, "Merging belief propagation and the mean field approximation: a free energy approach," *IEEE Transactions on Information Theory*, vol. 59, no. 1, pp. 588-602.
- [33] E. Nachmani, E. Marciano, L. Lugosch, W. J. Gross, D. Burshtein, and Y. Be'er, "Deep learning methods for improved decoding of linear codes," *IEEE Journal of Selected Topics in Signal Processing*, vol. 12, no. 1, pp. 119-131, Feb. 2018.
- [34] Z. Zhang, Y. Li, L. Liu, and W. Hou, "Fixed-symbol aided random access scheme for Machine-to-Machine communications," *IEEE Access*, vol. 7, pp. 52913-52928, 2019.
- [35] R. Razavi, A.-I. Mohammed, M. A. Imran, R. Hoshyar, and D. Chen, "On receiver design for uplink low density signature OFDM (LDS-OFDM)," *IEEE Transactions on Communications*, vol. 60, no. 11, pp. 3499-3508, Nov. 2012.
- [36] L. Wen, R. Razavi, P. Xiao, and M. A. Imran, "Fast convergence and reduced complexity receiver design for LDS-OFDM system," in *Proc. IEEE PIMRC*, Sept, 2014, pp. 918-922.
- [37] R. C. Frank and S. A. Zadoff, "Phase shift pulse codes with good periodic correlation properties (Corresp.)," *IRE Trans. Inf. Theory*, vol. 8, no. 6, pp. 381-382, Oct. 1962.
- [38] D. G. Tzikas, A. C. Likas, and N. P. Galatsanos, "The variational approximation for Bayesian inference," *IEEE Signal Process. Mag.*, vol. 25, no. 6, pp. 131-146, Nov. 2008.